AVO analysis of VSP and well log data

Craig A. Coulombe, Robert R. Stewart, and Michael J. Jones*

ABSTRACT

This study uses VSP and well log data to analyze the AVO response of a subsurface gas-saturated carbonate zone. Analysis of the well log data show that the gas-saturated zone is dolomitized with a porosity as high as 18 %. The VSP data consist of three surveys; a zero-offset VSP; an offset VSP, and a multioffset VSP. The P-SV converted-wave reflections from the offset VSP and multioffset VSP were found to correlate well with the pure P-wave reflections from each VSP. Forward modeling was used to analyze the AVO response of the gas-saturated zone. It was found that there is extreme tuning in the reservoir zone, causing the combined AVO response of the layers within 1/2 of the seismic wavelength to be very complicated. It was also found that a better match of the forward model data with the field multioffset VSP data could be made by lowering the P-wave velocity in the reservoir zone.

INTRODUCTION

Amplitude-versus-offset (AVO) analysis has been considered for some time as a useful exploration procedure (Ostrander, 1984; Chacko, 1989; Rutherford and Williams, 1989; Burnett, 1990). The main thrust of AVO analysis is to obtain an estimate of the Poisson's ratio in a subsurface zone using conventional surface seismic data. The principal interest in Poisson's ratio (or equivalently the *Vp/Vs* ratio) is that it may be diagnostic of both gas saturation and gross lithology (Tatham and Krug, 1985).

The theory behind AVO has been known for some time. The original papers deriving the equations for reflection and refraction of harmonic elastic waves at an interface between isotropic homogeneous elastic solids were published by C.G. Knott in 1989, and K. Zoeppritz in 1919 (Young and Braille, 1976). Early work in understanding these equations and hence understanding seismic reflection was done by Muskat and Meres in 1940. They concluded that reflected energy from various types of interfaces will decrease with increasing angle of incidence, but the effect's magnitude is small for the angles of incidence used (less than 10°). They use these findings to justify the assumption of normal incidence for offset traces. It should be noted that they assumed a constant Poisson's ratio of 0.25.

Koefoed (1955) tested the effects of varying the Poisson's ratio in the medium above and below an interface on the reflection amplitudes of planar P-waves. Koefoed's results are important when considering AVO. Koefoed derived several rules for the reflection coefficient versus angle of incidence curve that are summarized graphically in Figure 1. Koefoed also states that in the remote future, it may be possible to interpret the lithological nature of rock strata from the shapes of the reflection coefficient curves. This statement could be used today as a definition of AVO analysis.

* Schlumberger of Canada

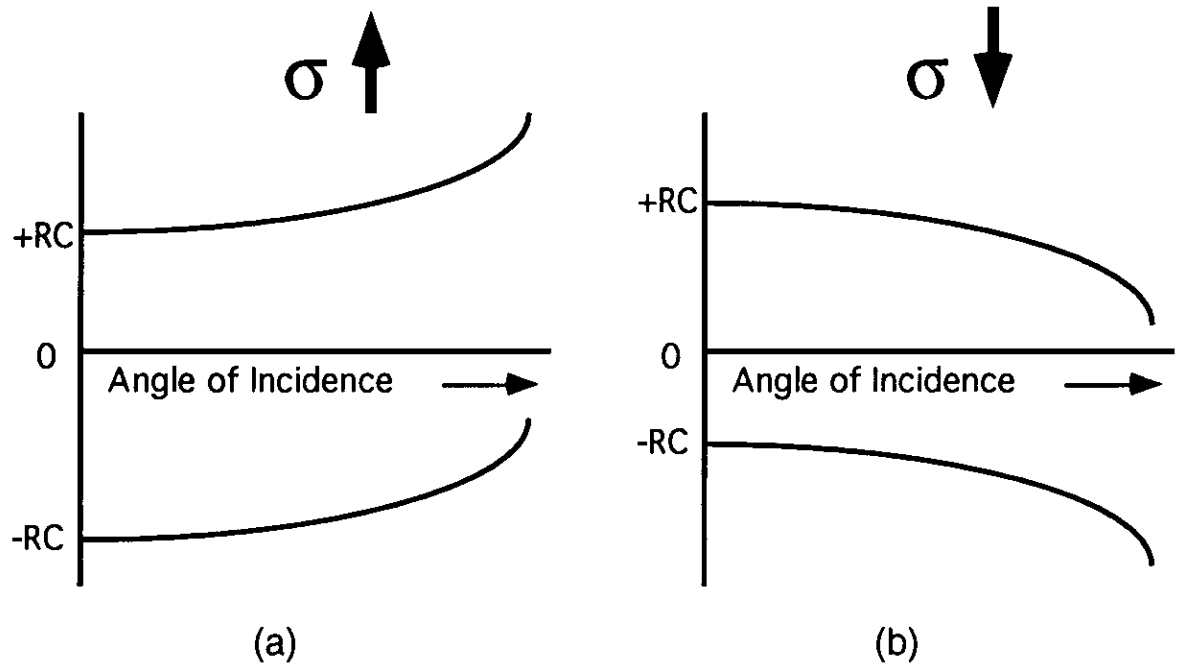

FIG 1. Reflection coefficient versus angle of incidence curves; (a) for an increase in Poisson's ratio (σ) across an interface, and (b) a decrease in Poisson's ratio across an interface.

Ostrander (1984) introduced a practical application of the AVO phenomenon. He used the Zoeppritz amplitude equations (e.g., Aki and Richards, 1980) to analyze the reflection coefficient versus angle of incidence curves for a simple three-layer, gas-sand model. The model consisted of a sand layer encased in two shale layers. By using published values of Poisson's ratio for shale, brine-saturated sandstone, and gas-saturated sandstone, he determined that there is a significant enough difference in reflection coefficient versus angle of incidence to discriminate between gas-saturated sandstone and brine-saturated sandstone. He tested his theoretical observations with field seismic data and determined that AVO can be used as a method of detecting gas sands.

Vertical Seismic Profiling

The VSP can be used to gain insight into wavefield propagation (Lee and Balch, 1983; Gaiser et al. 1984; and Dankbaar, 1987). The total seismic wavefield is recorded in situ over a number of depth levels. With this geometry upgoing and downgoing seismic events can be identified at different points of their propagation path in depth and time. Furthermore, many wavefield propagation effects can be observed: seismic attenuation can be measured by comparing the amplitude spectra of the downgoing wavefield at different depth levels; on offset VSPs both reflected and transmitted mode-converted S-waves can be observed (proving the Zoeppritz Equations); and multiples can be identified and removed. Thus using the VSP in interpretation and analysis generally leads to a well-defined solution that is independent of many of the uncertainties that plague surface seismic data.

Although there are many advantages in using VSP data, there are also limitations: a well must be available for VSP acquisition; VSP data are limited in subsurface coverage;

and the VSP may have a substantial cost. These factors are often acceptable when considering the quality and detail of the data that is acquired.

There are several aspects of the VSP that can be used to an advantage when considering AVO. The downgoing wavefield is recorded, and can be used to design a deconvolution operator that eliminates many of the wavefield propagation effects (such as multiples) between the source and receiver. Essentially, the downgoing wavefield can be shaped to a desired wavelet of known phase. The operator used to shape the downgoing wavefield is then applied to the upgoing wavefield, and the result is the reflection coefficient series convolved with the desired wavelet as shown by Gaiser et al. (1984). Additionally, the amplitudes of the seismic wavefield are recorded, and can be used to obtain a good estimate of the reflection coefficient of an interface by taking the ratio of the incident and reflected amplitudes. A similar technique was also used recently by Cheng et al. (1992). Reflection coefficients were measured using the VSP many years ago by Jolly (1953). Furthermore, the incident and reflected amplitudes can be measured immediately above the interface, eliminating most wavefield propagation effects, and resulting in the true amplitude seismic response. Another aspect of the VSP is that three-component acquisition and processing can be used to obtain mode-converted P-SV reflections. This suggests that P-P and P-SV reflections can be used jointly in an AVO study to help understand the subsurface rock parameters. Thus the additional information in the converted wave reflections should enhance the interpretation and analysis of the seismic wavefield.

So, in summary the main advantages of the VSP are that the seismic reflections are measured in situ where they occur, resulting in the possibility of true amplitude seismic processing, the seismic wavelet is known, and the data can be processed to be largely multiple free. Also, VSP data generally have a higher bandwidth than comparable seismic data due to the shorter travel path, and the signal to noise ratio is generally higher than surface seismic data due to the quite borehole environment and strong borehole coupling.

VSP Geometry for AVO Analysis

A multioffset geometry (Figure 2) is used in this study to record data specifically for AVO analysis of a particular interface or reservoir zone. The fundamental aspects of this geometry are the source and receiver positions. Several source positions are located at increasing distances (offsets) from the borehole to obtain seismic reflections for a range of P-wave angles of incidence. A number of 3-component geophones (receivers) are placed immediately above the zone of interest. These geophone locations cause the reflection point from a given interface to remain near the borehole, and thus approximately the same point in the subsurface is imaged by all the source positions. The true seismic amplitudes can be obtained by taking the ratio of the incident and reflected wave amplitudes. As shown schematically in Figure 2, the two seismic events diagrammed; a P-wave direct arrival and a P-wave reflection, are recorded by the geophone . When the geophone is near the interface, the amplitude of the recorded P-wave direct arrival and the amplitude of the P-wave incident on the interface are approximately equal. So, the ratio between recorded upgoing and downgoing P-wave events is the P-P reflection coefficient of the interface. The ratio is independent of most wave propagation effects (attenuation, transmission losses, multiples, and spherical spreading) because the travel path of the reflected wave is small, and the travel paths of the two downgoing P waves are nearly the same. Also with this geometry it is necessary to record at several depth levels above the interface to accommodate multichannel wavefield separation algorithms required to separate the seismic wavefield into the different propagation modes.

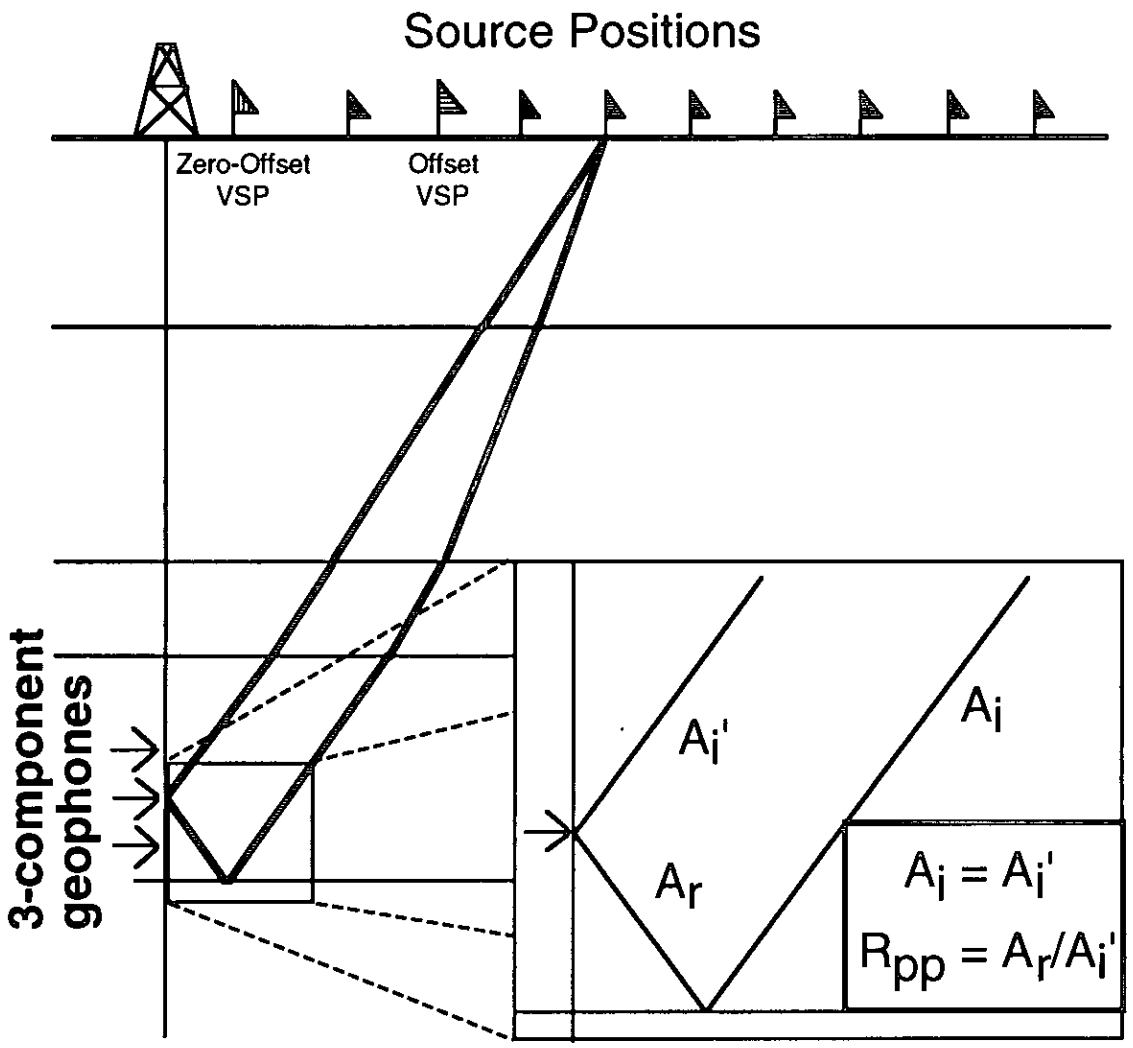

FIG 2. AVO VSP geometry outlining the positions of the sources and the receivers. The positions of the sources for the zero offset and offset VSPs are also displayed.

VSP Acquisition

The source positions of the VSP survey are shown in plan view in Figure 3. The receiver positions are outlined in Table 1 for each VSP survey type. The target depth for the survey is approximately 2500 m. The receiver was a single-level 3-component mechanically-clamped geophone. The data were acquired in open hole conditions (i.e., the borehole was not cased). The source was two Mertz-25 vibrators with a 12 s sweep from 10 to 90 Hz. The logistics of the survey were to acquire all the receiver positions for a given source position, and then move the source to the next position.

Table 1. Well A geophone locations.

Source Offset (m)	Number of Levels	Bottom Level (m)	Top Level (m)	Level Spacing (m)
80	75	2625	400	25
500	11	2525	2325	20
750	81	2525	905	20
1000	11	2525	2325	20
1250	11	2525	2325	20
1500	11	2525	2325	20
1750	11	2525	2325	20
2000	11	2525	2325	20
2250	11	2525	2325	20
2500	11	2525	2325	20

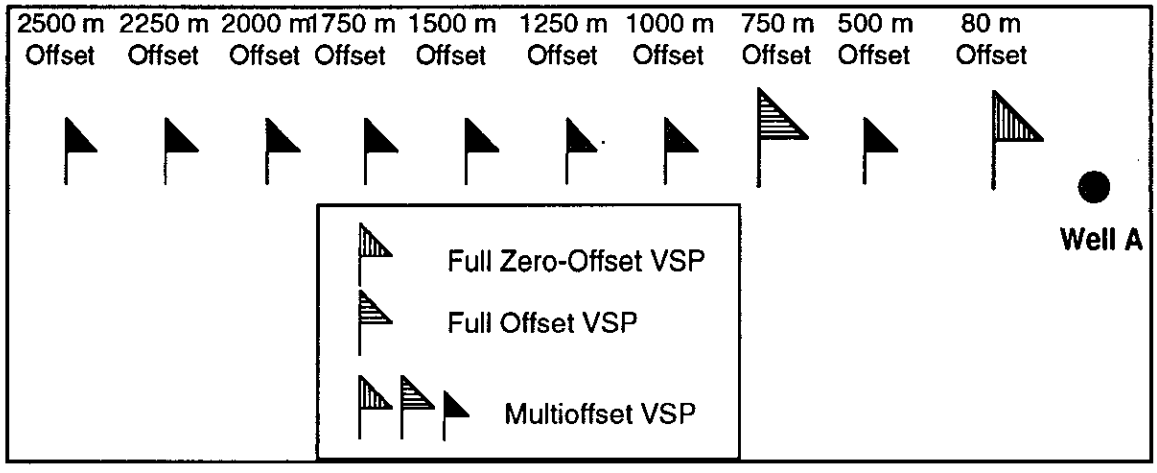

FIG 3. Schematic plan view of the Well A VSP survey geometry. Three VSP surveys are diagrammed; a zero-offset VSP at 80 m from the borehole, an offset VSP at 750 m from the borehole, and a multioffset VSP with 10 offsets ranging from 80 to 2500 m from the borehole.

Study Objectives

There are several objectives in this study. The main objective is to use the multioffset VSP geometry to understand the AVO behavior of a subsurface reservoir zone. In meeting the main objective, several smaller objectives such as VSP interpretation, well-log interpretation, AVO single interface forward modeling, and AVO multi interface forward modeling, must be met to form a basis for the underlying objective of this study. These smaller objectives lead to a clear understanding of the underlying goal of this study.

VSP INTERPRETATION

After processing the VSP data, the next step is interpretation. In this study, the well logs and the VSP data will be interpreted. The log interpretation involves blocking the

logs and interpreting the blocked logs for lithology. The VSP data interpretation is more complicated. First, the zero-offset VSP is interpreted using the synthetic seismogram generated from the well logs. The goal of this interpretation is to correlate the layers in the zone of interest from the well logs to the zero-offset VSP. Some issues to be addressed are the thin-bed interference effects and the VSP data polarity. Second, the zero-offset VSP is correlated with the offset VSP and the multioffset VSP. The purpose is to establish P-P and P-SV reflectivity correlations and to determine the polarity of the P-SV events. Third, the P-P and P-SV AVO responses of the multioffset VSP data are interpreted. The goal of this interpretation is to understand the AVO response of the reservoir zone and to determine how well the forward model data match the field data. So, the interpretation of these data is broad in scope. However the approach is to start with a basic interpretation of the zero-offset VSP and build up to the more complex AVO interpretation of the multioffset VSP.

Well A Log/Zero-Offset VSP Interpretation

To form a basis for the VSP well-log correlation, it is necessary to interpret the well logs. The well logs are interpreted to understand the lithology and petrophysical parameters, such as porosity, near the well bore. When comparing well logs with seismic data, it is important to determine the vertical resolution of the two measurements given the different frequency bandwidths of the data. A rough calculation of the seismic wavelength is made by looking at the waveshaping-deconvolved downgoing P wavefield from the zero-offset VSP. These deconvolved traces are approximately the VSP wavelet, and the period of this wavelet is about 20 ms (trough to trough time). A 20 ms period corresponds to a frequency of 50 Hz. Given that the zone of interest is a carbonate, an average velocity of carbonate rocks of 5500 m/s is used. The seismic wavelength (λ) is calculated to be $\lambda=v/f=5500/50=110$ m. Seismic resolution is defined to be about 1/8th of a wavelength (Widess, 1973), and 1/8th of the seismic wavelength in this case is 13.75 m. This suggests that any beds thinner than about 13 m will be unresolvable. Sonic-logs have a vertical sampling interval of less than 1 m. So, there is a large discrepancy between the vertical resolution of the well log and VSP data.

Well A Log Blocking

The goal of this study is to recover the elastic parameters from the VSP AVO response of the reservoir. So, the first problem in the interpretation is to find a common layering of the Earth that satisfies both the well logs and the VSP data. A common method of addressing this problem is to average (block) the logs into larger depth intervals. The result of this log-blocking step is a simplified Earth model that retains the coarse information in the well logs, but dismisses the fine information that is unresolvable with seismic data. The simplified Earth model is also desirable as a starting point for the Generalized Linear Inversion algorithm that will be introduced layer. The main requirement of the log blocking is that the blocked logs retain enough information for a good correlation of the synthetic seismogram generated from the blocked logs and VSP data. This implies that the significant seismic events are retained in the blocked logs.

The raw logs to be used for the VSP interpretation are the full-waveform sonic and bulk density logs. The full waveform sonic logs measure the compressional and shear wave slowness while the bulk density log measures the electron density of the rocks that is related to the bulk density. The raw sonic and density measurements in the zone of interest are shown in Figure 4. Notice that these measurements have a very fine sampling interval of less than 1 m. These logs are blocked using a compound median filtering technique (Leaney and Ulrych, 1987). This technique is automatic so there is no bias introduced by the interpreter. The technique uses a series of median filters starting with a filter width of three and ending with a filter width of 1/2 the maximum bed thickness. A maximum filter

width of 25 m was used to filter the data. A comparison of the logs before and after median filtering is shown in Figure 5. Note that the median filtered logs have the main characteristics of the raw logs, but have little of the fine detail in the raw logs. The logs are now simplified and can be interpreted for gross lithology.

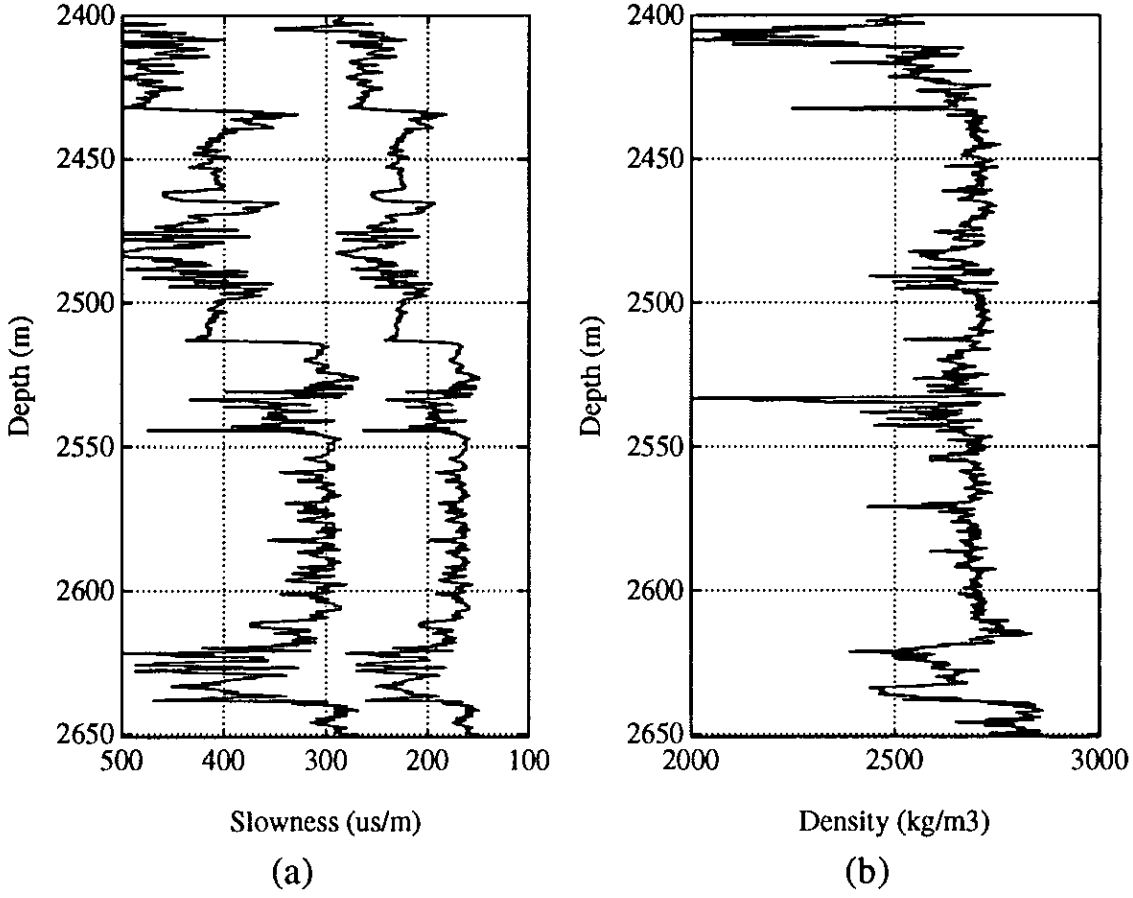

FIG. 4. Raw well logs in zone of interest (a) full waveform sonic log with compressional wave and shear wave slowness curves, and (b) bulk density log with bulk density curve.

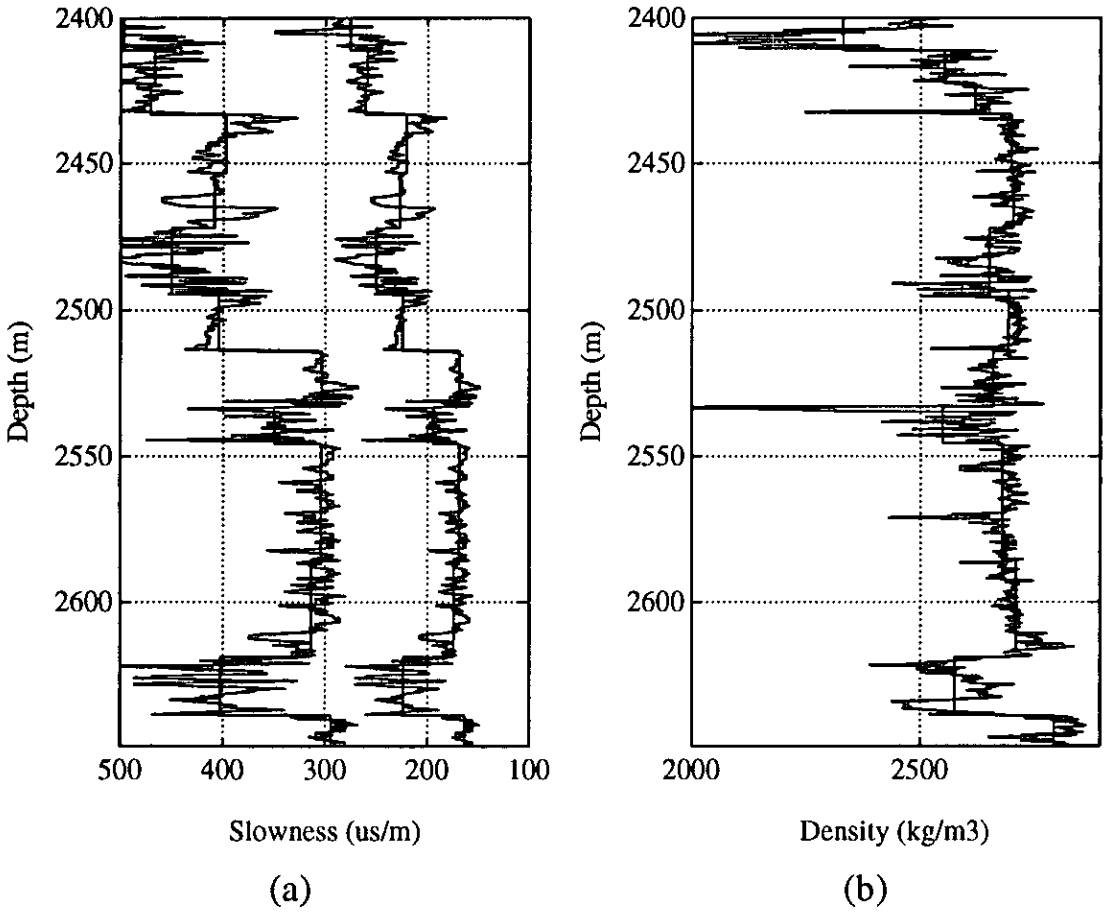

FIG. 5. Raw and blocked well logs in zone of interest; (a) full waveform sonic log with compressional wave and shear wave slowness curves before and after log blocking, and (b) bulk density log with bulk density curve before and after log blocking.

Well A Log Interpretation

The blocked well logs now represent the average elastic properties of the rocks. The zone of interest in Well A is at a depth of about 2530 m. Note in Figure 5 that all three of the log curves decrease in this zone. The zone has been tested and is proven to be gas saturated. For the lithology interpretation, the zones above and below the gas zone will also be analyzed. The blocked-log measurements for the 3 zones are listed in Table 2.

Table 2. Average log values in zone of interest.

Zone	P-wave Slowness (μs/m)	S-wave Slowness (μs/m)	Bulk Density kg/m^3
Upper zone	167	314	2660
Gas zone	193	337	2550
Lower zone	166	316	2688

The measurements shown in Table 2 can be used to determine the porosity and lithology of these zones by comparing cross plots of the P-wave transit time and the bulk

density with published log-interpretation charts (Schlumberger, 1988). The upper zone cross plots as a limestone with 2.5 % porosity, the gas-zone cross plots between a limestone with 10 % porosity and a dolomite with 17 % porosity, and the lower zone cross plots as a limestone with 2 % porosity.

Figure 6 shows the raw photoelectric cross-section curve through the zone of interest. The photoelectric cross section log responds primarily to lithology and secondarily to porosity and pore fluid (Schlumberger, 1987). Limestone generally has a photoelectric cross section of about 5 Barns/electron and dolomite generally has a photoelectric cross section of about 3 Barns/electron. The log curve in Figure 6 has a sharp decrease in photoelectric cross section at a depth of 2530 m corresponding to the top of the reservoir. The photoelectric cross section log is approximately 3 barns/electron in the reservoir zone between 2530 m and 2545 m, suggesting the zone is dolomite. The layers above and below the reservoir zone have values of 5 barns/electron, suggesting these zones are limestone. So, because the photoelectric cross section log responds primarily to lithology, the reservoir zone is dolomite, and the layers above and below are limestone. The photoelectric cross section log can also be cross plotted against bulk density. The upper zone cross plots as a limestone with 2 % porosity, the reservoir zone cross plots as a dolomite with 17 % porosity, and the lower zone cross plots as a limestone with 1 % porosity.

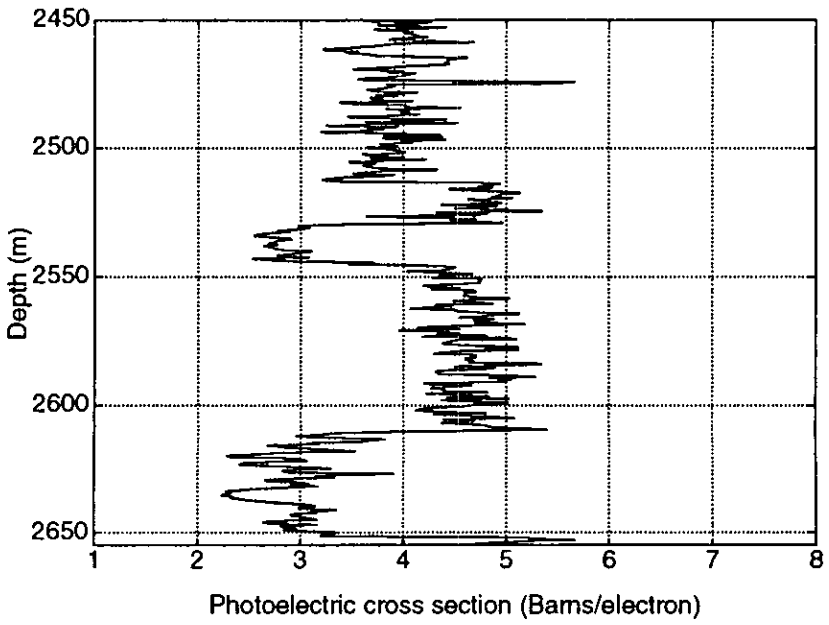

FIG. 6. Photoelectric cross section log through zone of interest.

Once the lithology is established, the bulk density log can be used alone to calculate the porosity. Assuming the bulk density tool measures mainly the response of the invaded zone, the porosity can be calculated using a porosity weighted average equation (Sclumberger, 1987)

$$\phi = \frac{\rho_{ma} - \rho_b}{\rho_{ma} - \rho_f} \times 100\%, \qquad 3.1$$

where ρ_{ma} is the matrix density, ρ_b is the measured bulk density, and ρ_f is fluid density. The fluid density was 1.1 g/cm^3, the matrix density for dolomite is 2.870 g/cm^3, and the matrix density is 2.710 g/cm^3 for limestone. So inputing the bulk densities in Table 2 into equation 3.1 results in porosities of 3 % for the upper zone, 18 % for the gas-zone, and 1 % for the lower zone.

Several methods have been used to determine the lithology and porosity of the reservoir zone. There are uncertainties in some of the log measurements due to the presence of gas in the reservoir. However, the photoelectric cross section log discriminates very well between dolomite and limestone and thus the reservoir is clearly a dolomite encased in limestone. The limestone units have very low porosity, and the reservoir dolomite has a high porosity possibly as high as 18 %.

The next stage of the interpretation is to compare the measured sonic velocities with the VSP velocities. The VSP velocities are determined using a traveltime inversion algorithm similar to Stewart (1984). The first-break traveltimes from the zero-offset VSP were used to invert for the P-wave velocities, and the traveltimes from a downgoing S-wave event on the offset VSP were used to invert for the S-wave velocities. In both cases the blocked-sonic log velocities were used as an initial guess for the inversion algorithm. A comparison of the blocked-sonic and VSP velocities is shown in Figure 7. Note that there is a constant V_P/V_S ratio for the sonic log above the upper limestone layer. This is because the full-waveform sonic log was only acquired below this depth. Thus the sonic S-wave transit times were estimated from the P-wave transit times above this depth using a constant V_P/V_S ratio of 1.88.

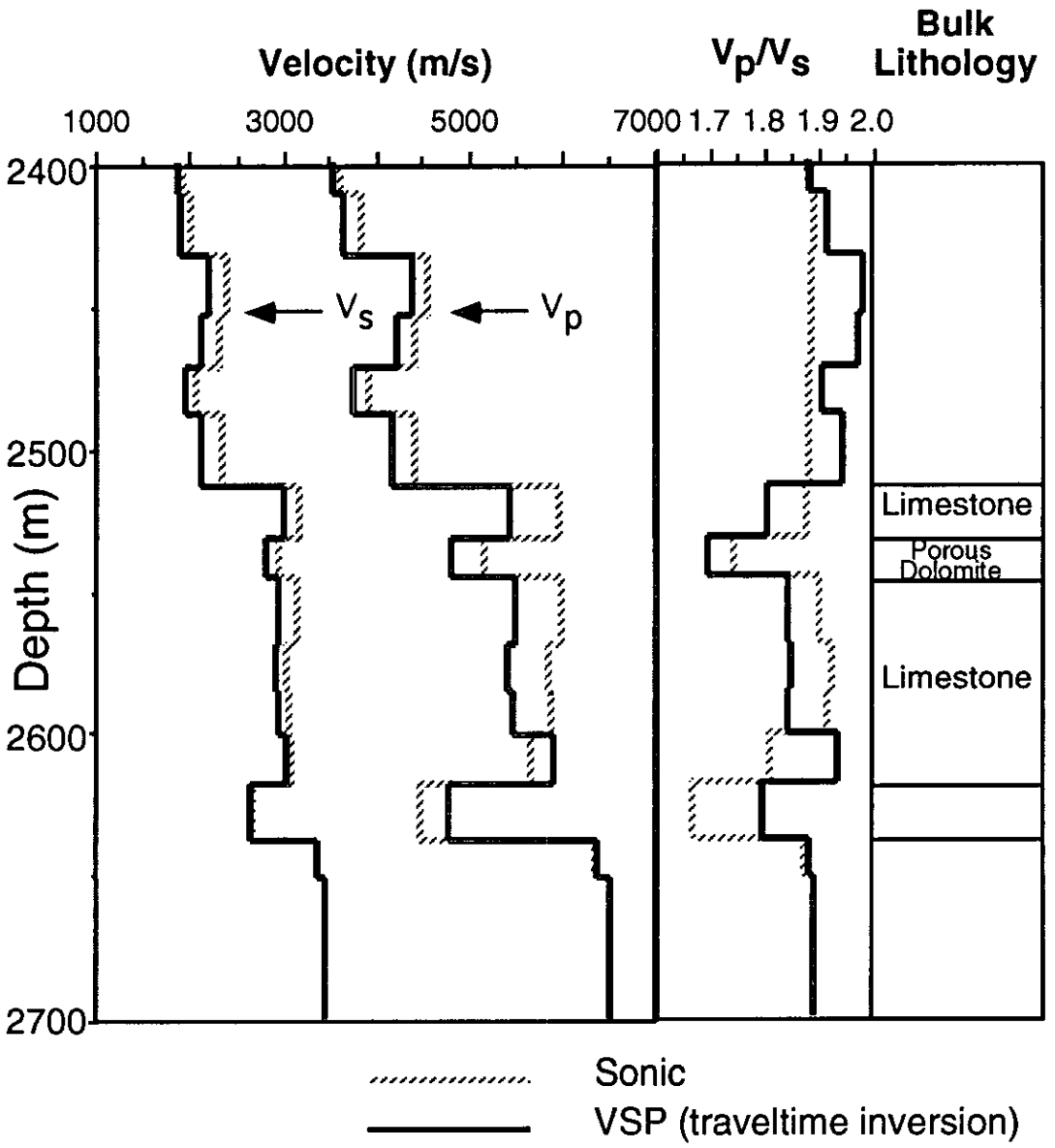

FIG. 7. Blocked-sonic and VSP velocities, V_P/V_S ratio, and bulk lithology from Well A. The zone of interest is at approximately 2520 m where there is a large decrease in the V_P/V_S ratio.

The comparison of the sonic and VSP velocities shows that the VSP velocities are generally lower than the sonic velocities. It is well documented (Stewart et al., 1984) that VSP velocities are generally lower than sonic velocities due to velocity dispersion. The VSP data have a lower bandwidth than the sonic logs (10-70 Hz compared with ≈10,000 Hz), and because of dispersion generally have lower velocities. The VSP velocities will be used for further analysis because these velocities are determined using the same frequency band that is in the seismic reflections.

VSP/Well Log Correlation

The 1-dimensional (1-D) seismic response of the VSP velocity model can now be compared with the corridor stack from the zero-offset VSP. A favorable comparison suggests that the velocity model is an accurate representation of the Earth in a 1-D sense, and that the layering of the model, based on the well logs, is valid. An unfavorable comparison suggests that either the layering of the model or the acoustic parameters of the model are in error. So, the correlation of the 1-D synthetic seismogram with the VSP corridor stack is an important test to the methods used in this analysis, especially the log blocking.

The 1-D synthetic was created using the convolutional model. The polarity of the synthetic seismogram was calculated such that a positive reflection coefficient or impedance increase results in a positive peak when convolved with the wavelet. Both the bulk density and P-wave velocity were used to calculate the acoustic impedance and hence the reflection coefficients. The reflection coefficients were transformed to time and then convolved with the VSP wavelet. The VSP wavelet was extracted from the waveshaping deconvolved downgoing P wavefield and scaled to a peak amplitude of 1.0. A comparison of the VSP corridor stack and the synthetic seismogram is shown in Figure 8. Note that the amplitudes and seismic character match reasonably well. No scaling has bee applied to the corridor stack, so the zero-offset VSP data have been processed to true amplitudes. The good match between the synthetic seismogram and the VSP corridor stack suggests that the Earth model is valid in the 1-D of the well bore.

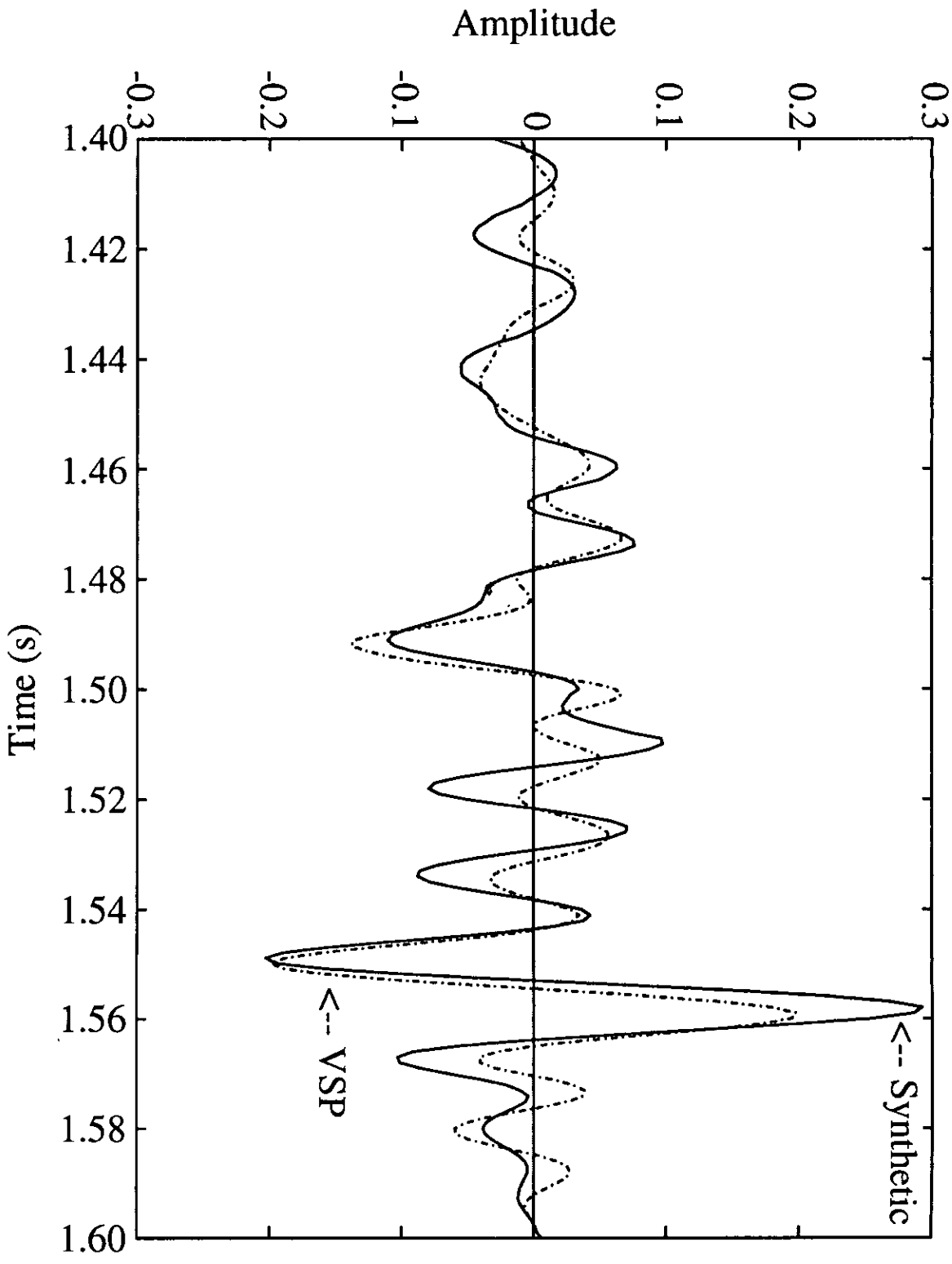

FIG. 8. Comparison of the synthetic seismogram generated from the blocked VSP P-wave velocity and blocked bulk-density log and the VSP corridor stack trace. The synthetic trace is solid and the VSP trace is dashed.

A good correlation has been established between the VSP corridor stack and the synthetic seismogram from the well logs. So, the VSP can now be correlated with the well logs using the synthetic seismogram. A first step in this analysis is to transform the well logs to time. Because the P-wave well log curve has been corrected using the VSP travel times, it can be used to calculate the time-depth curve used to transform the well logs to time. The logs in time are shown in Figure 9. The zone of interest is between approximately 1.51 and 1.53 s.

By overlaying the reflection coefficient time series on the synthetic seismogram and VSP corridor stack traces (Figure 10a), the exact timing of the seismic interfaces can be determined. This type of display also shows how the events are corrupted by wavelet interference (tuning). To correlate the reflection coefficients back to the well logs, the acoustic impedance curve is also plotted at the same scale in Figure 10b. This display shows that the top of the limestone unit (at approximately 1.515 s) has a positive reflection coefficient which correlates with a peak on the seismic traces. The top of porosity unit is a decrease in impedance resulting in a negative reflection coefficient that correlates fairly closely with a trough on the seismic traces. The base of the porosity unit has a positive reflection coefficient correlating approximately with a peak on the seismic traces. Note that the seismic waveforms in this interval exhibit thin bed effects. The peaks and troughs of the synthetic seismogram and VSP corridor stack do not correlate exactly with the reflection coefficients. This is caused by wavelet interference from events above and below the reflectors.

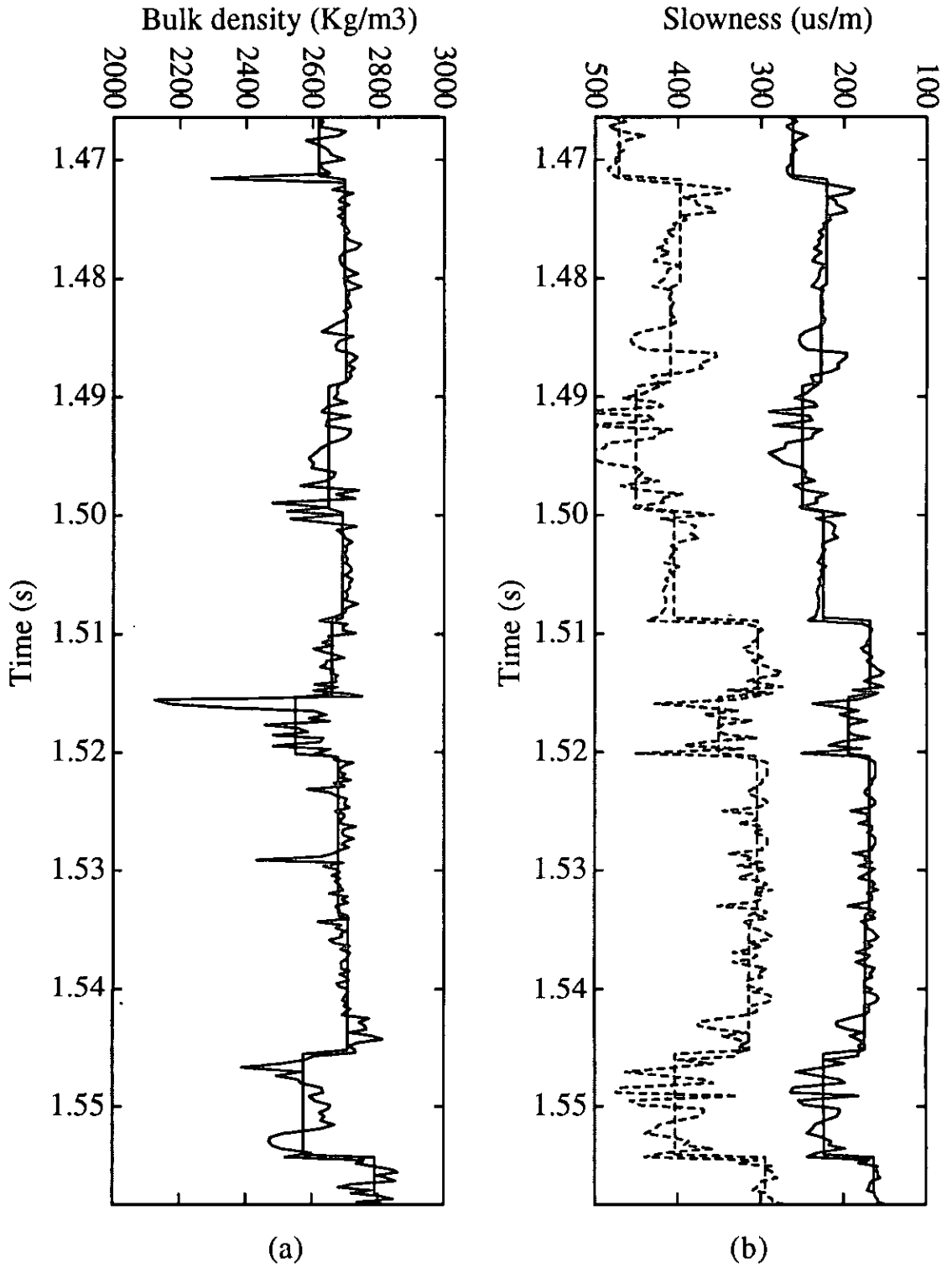

FIG. 9. Raw and blocked well logs in zone of interest transformed to time; (a) bulk-density log with bulk density curve before and after log blocking, and (b) full-waveform sonic log with compressional wave and shear wave slowness curves before and after log blocking.

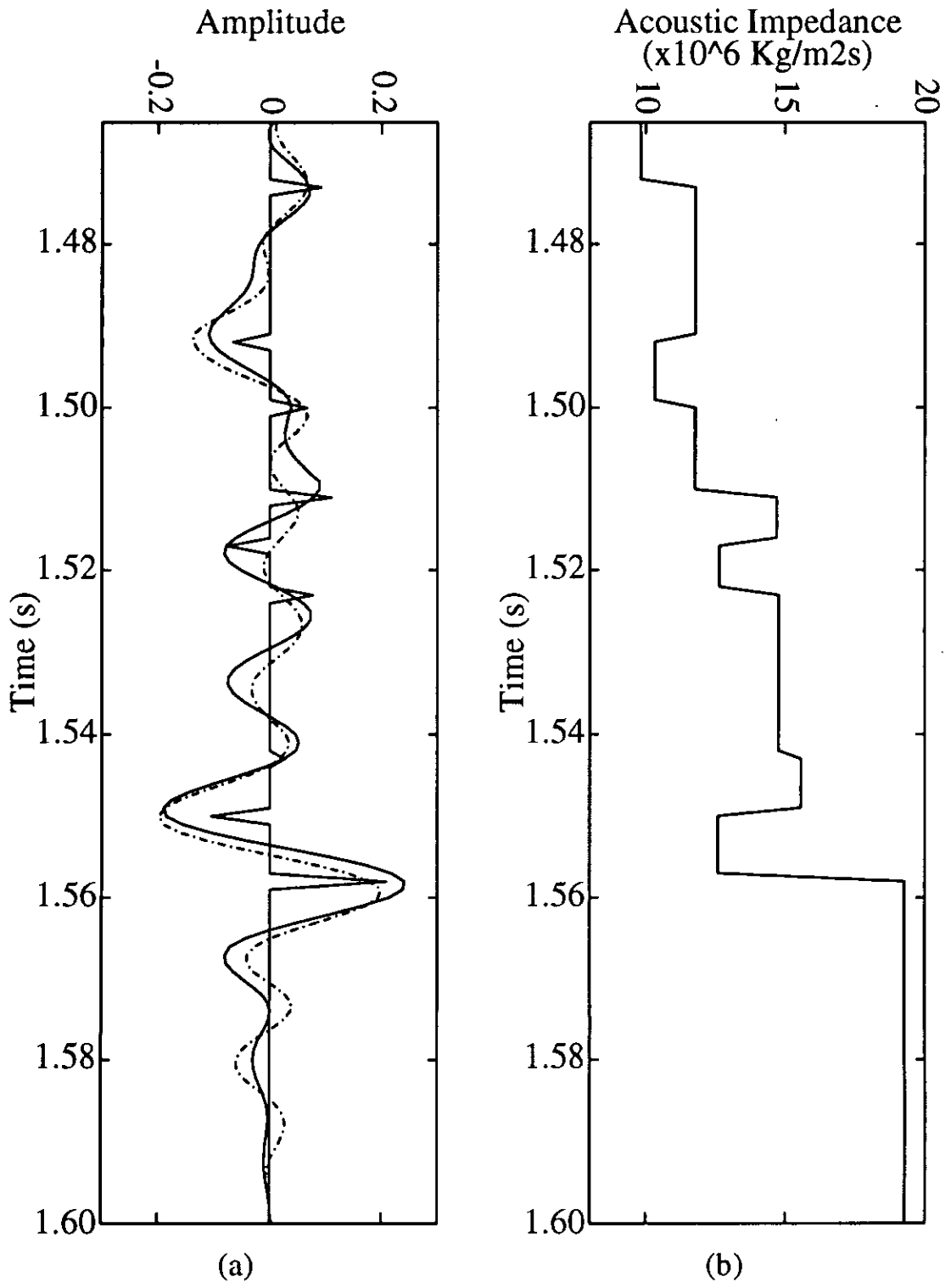

FIG. 10. Comparison of 1-D seismic with the acoustic-impedance log in time; (a) overlay of the reflection coefficient time series (spiked trace), synthetic seismogram (solid trace), and corridor stack (dashed trace), and (b) blocked acoustic impedance curve.

This interpretation has been limited to a very detailed analysis in the zone of interest, but there are other issues regarding the offset and multioffset VSPs that must be

addressed. In particular, the correlations between the well logs, zero-offset VSP, offset VSP and multioffset VSP. One of the main issues for this part of the analysis is the correlation between the P-P and P-SV reflections on the offset and multioffset VSPs.

Integrated VSP Interpretation

Both the offset and multioffset VSP surveys have been processed for P-P and P-SV reflections. The VSP has been shown to be a good domain to correlate these reflections (Geis et al., 1990). The VSP yields a time-depth curve that can be used to correlate P-P and P-SV reflections with well logs. This correlation can also be used to determine the polarity of the seismic data.

An L plot of the zero-offset VSP, corridor stack, and the sonic log is shown in Figure 11. Event 1 correlates with a decrease in slowness (increase in velocity) on the sonic log, resulting in a positive reflection coefficient. The corresponding event on the zero offset VSP is a positive peak, and therefore the polarity of the VSP data is normal. That is, a positive peak represents an increase in impedance. Event 2 correlates with an increase in slowness on the sonic log corresponding to a trough on the zero-offset VSP. Event 3 correlates with an increase in slowness on the sonic log corresponding to a trough on the zero-offset VSP. Event 4 and Event 5 both correlate with decreases in slowness on the sonic log corresponding to peaks on the zero-offset VSP. Event 5 is the top of the limestone unit that overlays the porous limestone reservoir. So, using the VSP and sonic log to correlate events has resulted in an unambiguous interpretation of the seismic events and the polarity of the zero-offset VSP data.

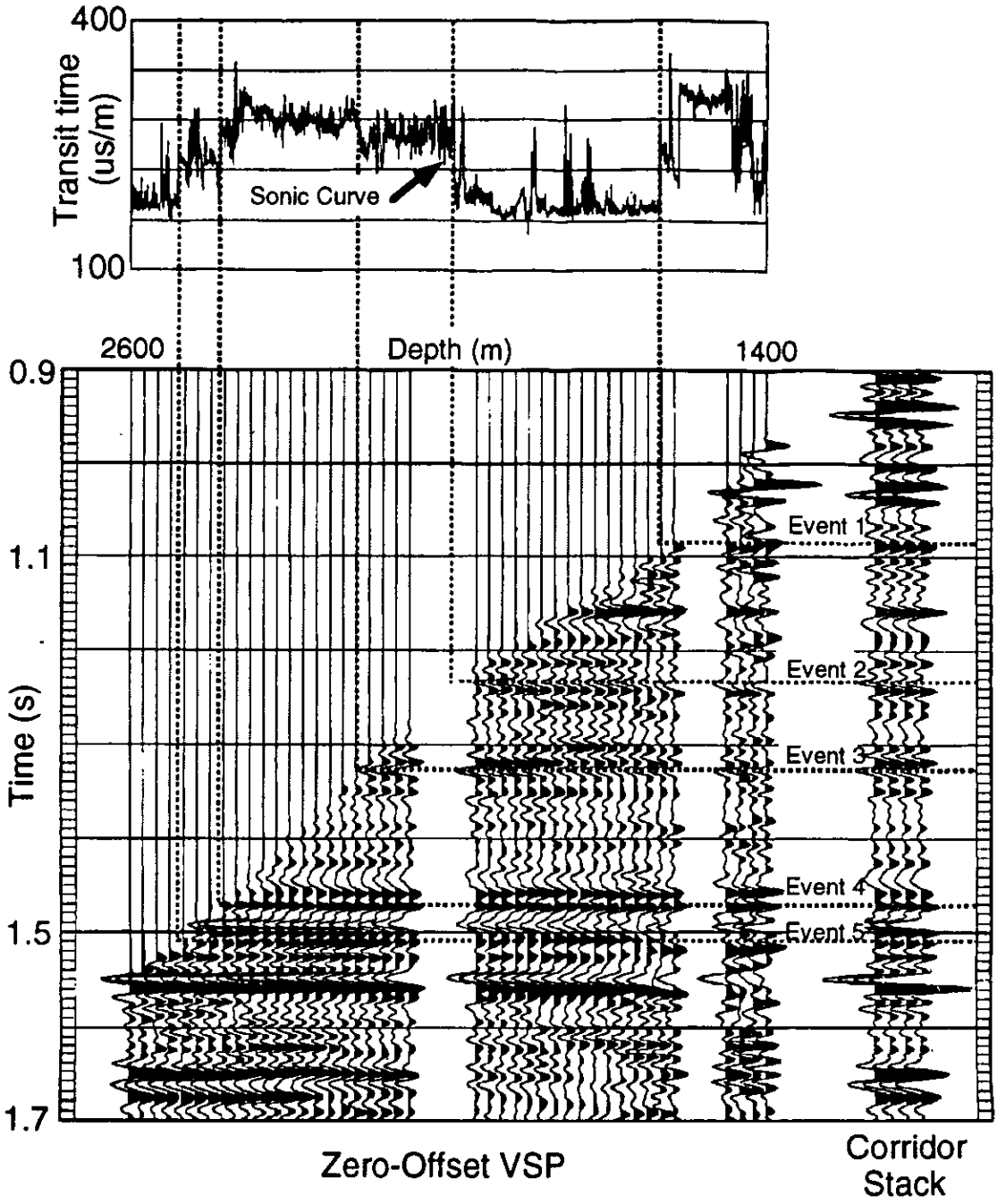

FIG. 11. L plot of sonic log, zero-offset VSP, and the zero-offset VSP corridor stack showing correlations of 5 events from the sonic log recorded in depth with the VSP recorded in time.

The correlation between the zero-offset VSP corridor stack, the multioffset P-wave gather, the offset VSP P-wave corridor stack, the multioffset S-wave gather, and the offset VSP S-wave corridor stack is shown in Figure 12. The correlation is generally good, however there are some interesting observations. The correlation of the offset VSP S-wave corridor stack with the zero-offset VSP corridor stack is better than the correlation of the offset VSP P-wave corridor stack with the zero-offset VSP corridor stack. This can be explained by the offset P-wave data having a lower frequency band than the zero-offset

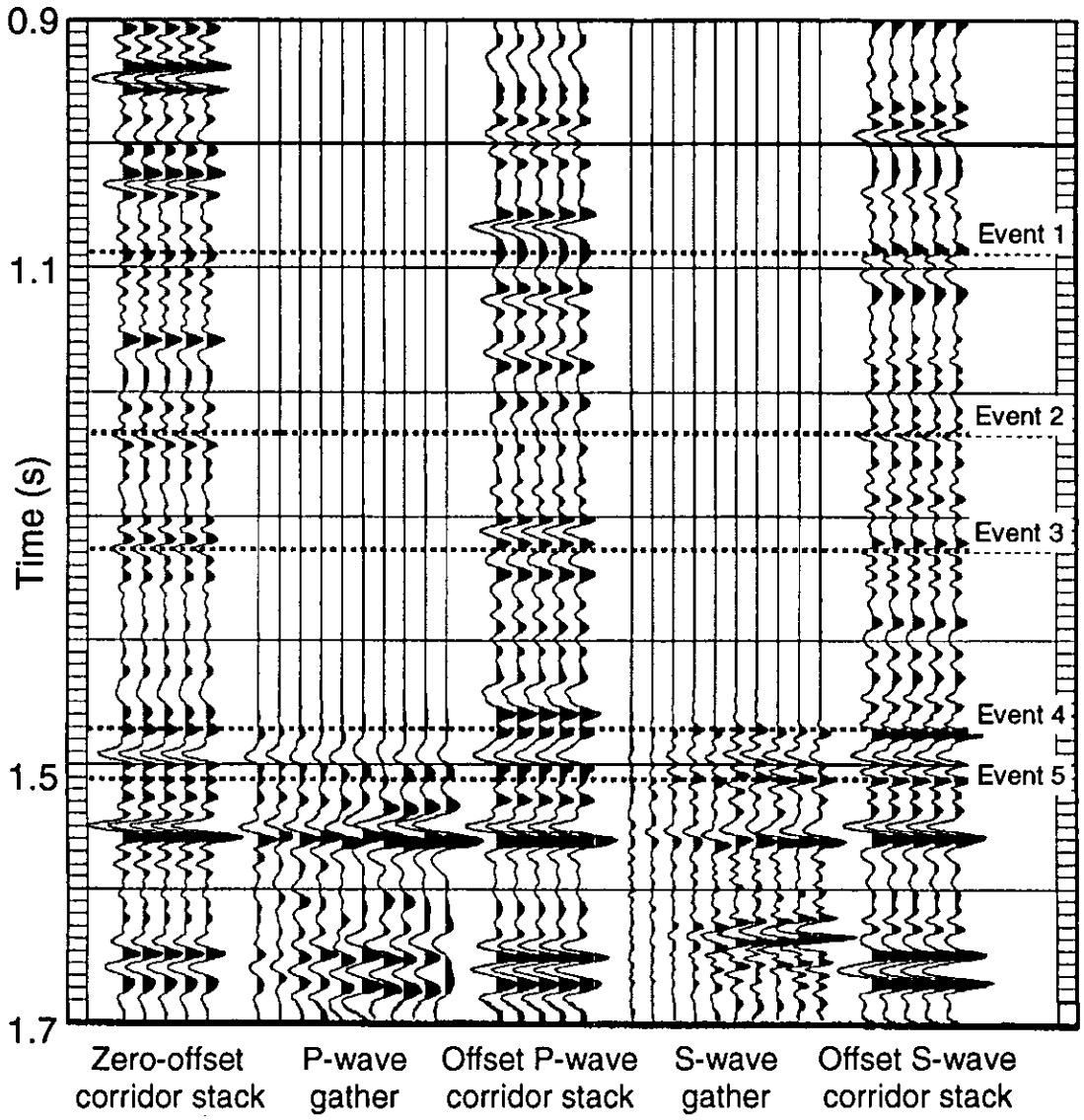

FIG. 12. Correlation of 5 Events across the VSP corridor stack, the P-wave gather, the offset VSP P-wave corridor stack, the S-wave gather, and the offset VSP S-wave corridor stack.

corridor stack and a longer wavelength than the offset S-wave data. The travel path for the offset VSP traces are longer than the travel-path for the zero-offset VSP traces, so it is reasonable that the longer travel path traces have lower frequencies due to attenuation and other propagation effects. The polarity of the converted-wave data (the S-wave gather, and offset VSP S-wave corridor stack) is such that an increase in S-wave impedance correlates with a trough. This is considered reverse polarity using the Aki and Richards (1980) convention .

AVO INTERPRETATION AND MODELING

The multioffset VSP data have been acquired and processed for AVO analysis. A first step in understanding the AVO response of the reservoir zone is to calculate the single

interface Zoeppritz equation solution for some of the events near the reservoir. This step is important to understand the individual AVO response of each of the layers in the reservoir zone. The next step is to calculate the multilayer forward model of the reservoir zone. This step is important to understand the offset dependent tuning effects.

For the single interface AVO modeling, the Zoeppritz equations for P-P and P-SV displacement have been solved for the top of the limestone interface, the top of porosity interface, and base of porosity interface. The VSP velocities and bulk densities were used as the input parameters. The results of these calculations are shown in Figure 3.9. These curves are plotted such that a phase term of 0° results in no change in the amplitude sign, and a phase term of ± 180° results in a reversal of the amplitude sign. Note that in each case the P-SV reflection coefficient is zero at normal incidence, increasing to a peak at an intermediate angle, and then dropping in amplitude at the larger angles of incidence as is expected. The top of the limestone interface P-P reflection coefficient curve (Figure 3.13(a)) has a decrease in amplitude with angle up to an angle of about 35°, and then has a strong increase in amplitude at the larger angles due to the critical angle. The top of porosity event P-P reflection coefficient curve (Figure 3.13(b)) has an increase in amplitude with angle response due to the decrease in V_P/V_S ratio with a positive normal incidence reflection coefficient. The base of porosity event reflection coefficient curve (Figure 3.13(c)) shows an increase in amplitude with angle response due to the increase in V_P/V_S ratio with a negative normal incidence reflection coefficient.

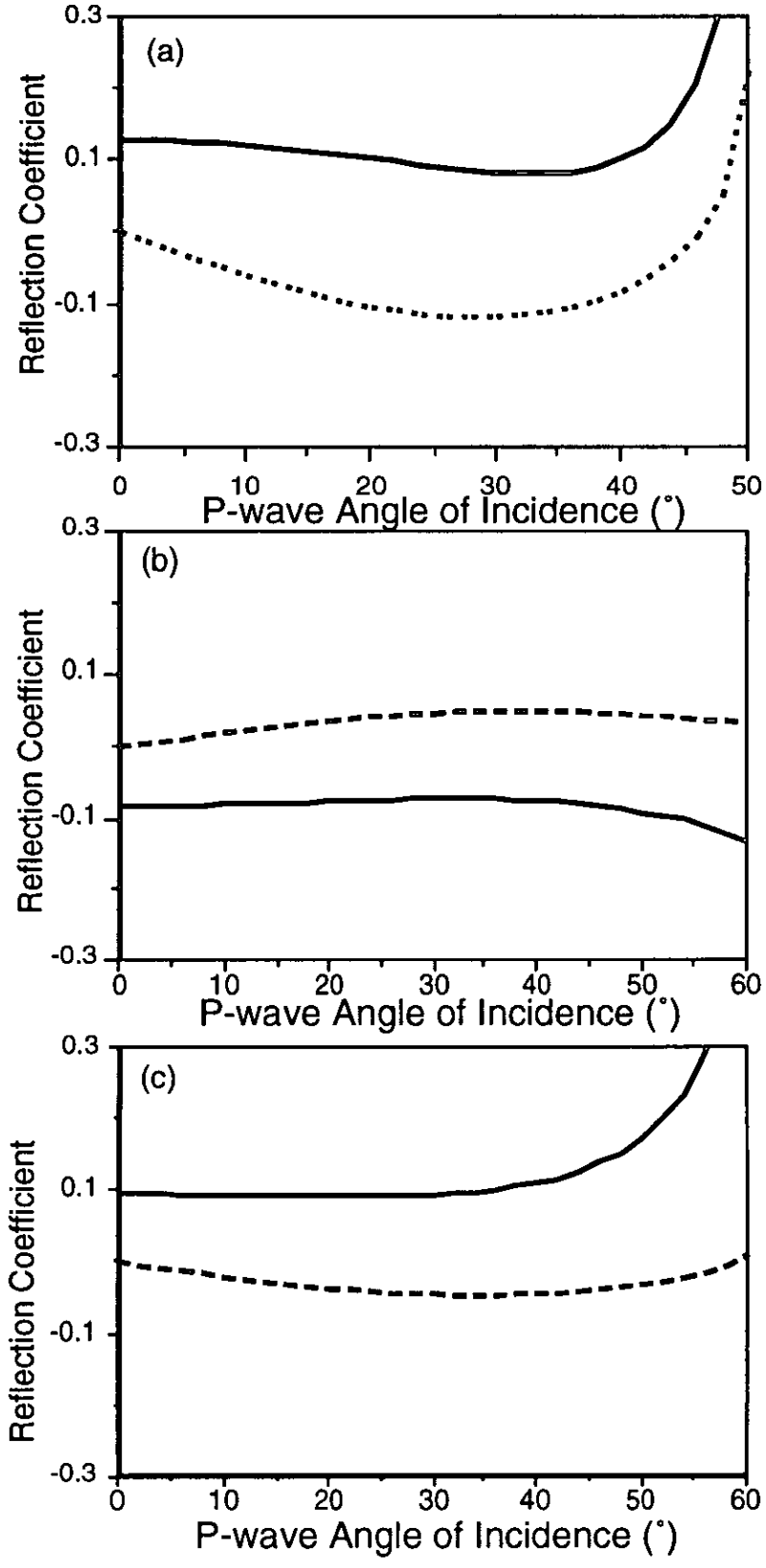

FIG. 13. Single Interface Zoeppritz equation solution for P-P (solid) and P-SV waves (dashed); (a) top of limestone interface, (b) top of porosity interface, and (c) base of porosity interface.

For clarity, an increase in amplitude with angle response is used here to signify that the absolute amplitude of the reflection coefficient increases at the larger angles of incidence. This means that a positive reflection gets larger in a positive sense, and a negative reflection gets larger in a negative sense. So, both the reflection coefficient curves for the top and bottom the porous limestone unit are consistent with Koefoed's rules.

Unfortunately for AVO analysis, seismic data are bandlimited so the seismic response from a particular interface is complicated by wavelet interference from surrounding events. Generally, there is wavelet interference from beds that are less than half a wavelength away. Therefore, because the reservoir thickness is less than half the seismic wavelength it is necessary to model the seismic response from all the layers near the reservoir zone. The forward model data were generated by ray tracing through the VSP velocity model, solving the Zoeppritz equations for the reflectivities, convolution with a zero-phase Ricker wavelet, and then NMO correction using the same algorithm that was used for the real data. For tuned events, it is important to include NMO in the modeling to account for the wavelet stretch that is in the real data. The effects of wavelet stretch have been quantified in other work (Ostrander, 1984; Swan, 1990) and this study reinforces how important this effect is for field data AVO analysis. The correlation of the P-P and P-SV forward models with the field P-P and P-SV gathers are shown in Figure 3.14. The two-way P-wave traveltimes of the top of limestone, top of porosity, and base of porosity events are also drawn (dahsed lines) on this plot. Generally, the correlation between the field and the model data is good, with the P-SV correlation being slightly better than the P-P correlation. The modeled P-P data (Figure 3.14(b)) have a large peak at 1.56 s that has a very strong AVO effect. The size of this peak is much larger than the corresponding peak on the real data. This is a critical-angle effect that probably can not be handled properly with the modeling method used. So, because of the size of this peak, the other amplitudes of the events are scaled down making the amplitude correlation appear worse than it is.

The event correlations also show how extreme the wavelet interference (tuning) effects are in these data. The P-P data have the events at the near offset, but the correlation changes at the far offset. This suggests that the effect of tuning changes with offset. The P-SV data events correlate better across the range of offsets than the P-P events. The reflected S waves have approximately the same frequency band and travel at lower velocities than the P waves. Thus the S-waves have a shorter wavelength (or higher resolution) than the P waves. So, the tuning effects are smaller for the P-SV reflections than for the P-P reflections.

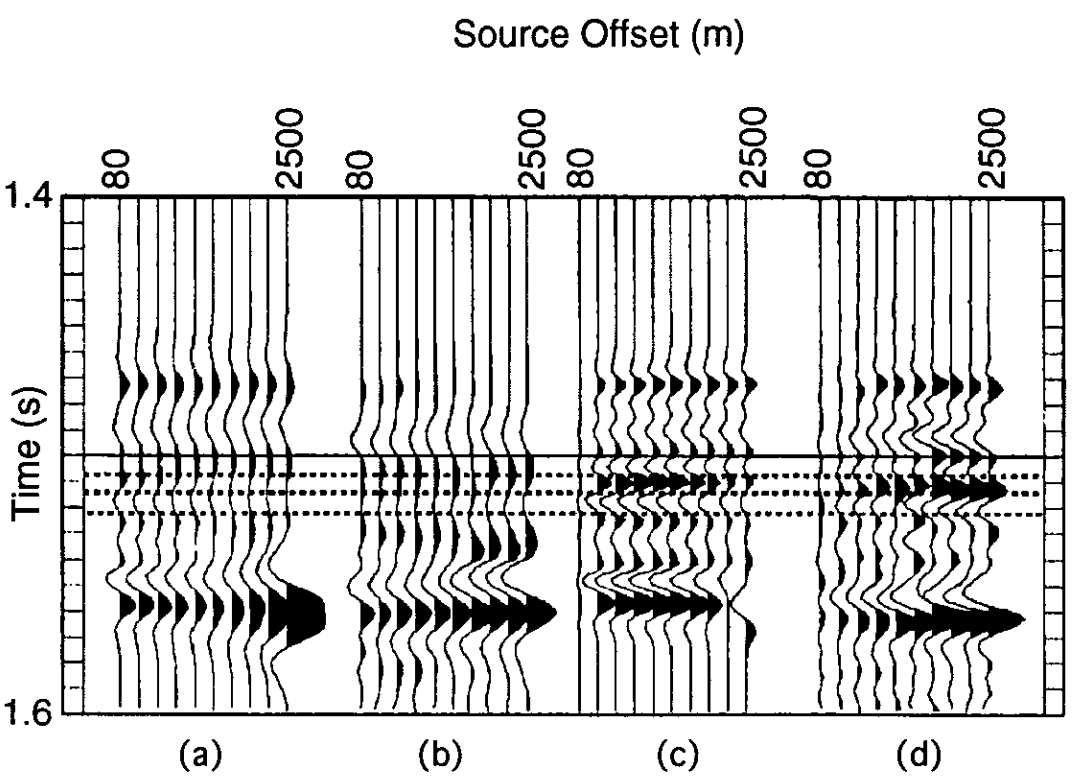

FIG. 14. Correlation of field (b) P-P and (d) P-SV gathers with multilayer forward modeled (a) P-P and (c) P-SV gathers. Three events (dashed lines) are correlated, the top event is the top of limestone interface, the middle event is the top of porosity interface, and the bottom event is the base of porosity interface.

The wavelet interference effects versus offset are complicated phenomena that affect the AVO response of the real and modeled P-P and P-SV data. One way of studying this effect is to model the interfaces independently, and then study the effects of adding the response of the different layers together. Figure 15 is a summary of this analysis for the P-P reflections. Each panel is an AVO model generated as previously, except fewer events are used. In Figure 15(a) only the top of the limestone interface is used for modeling. This event is highlighted in the schematic impedance profile plotted above the seismic response for reference. The hatched area of the impedance profile is the porous reservoir zone. So, Figure 15(a-c) are the AVO modeled responses of the top of limestone, top of porosity, and base of porosity interfaces respectively. Figure 15(d) is the AVO response from the top and base of porosity interfaces, and Figure 15(e) is the AVO response from all 3 interfaces.

The combined AVO response of the top and bottom of the porosity (Figure 15(d)) is approximately a 90° degree wavelet that is consistent with Widess (1973) for two tuned reflections of approximately equal strength but opposite polarity. So, the AVO response of these two interfaces is tuned, but it still shows a similar AVO response as the two individual interfaces (Figure 15(b) and Figure 15(c)). Interestingly, the AVO response from the top of porosity changes completely when the top of limestone event is included in the modeling (Figure 15(e)). The top of porosity AVO response changes from an increase in amplitude with offset to a decrease in amplitude with offset. Figure 15(f) is the AVO model of the same three interfaces plus the interface above the top of limestone. In this model response, the top of porosity event appears to have returned at the far offsets. However, this is likely side lobe interference from the additional event. The AVO response

from the base of porosity is relatively unchanged from the single interface response in this case.

Each of the remaining AVO model responses (Figures 15(g-k)) has one more lower event modeled than the previous model. The AVO response from the base of porosity changes considerably in Figure 15(i) and Figure 15(j). So, the AVO response from the base of porosity is also tuned and does not show the true AVO response of the individual event. In summary, this detailed AVO analysis shows that the AVO response of the reservoir zone is complicated by tuning effects that make it difficult to understand the exact AVO contribution of each layer independently.

Similar analysis has been carried out for the P-SV reflections and is shown in Figure 16. In this case, as discussed previously, these data have higher resolution than the P-P reflection data due to the shorter wavelength of the S waves. Therefore, there is less tuning in these data than in the P-P reflection data. Other differences besides the amount of tuning do exist. The AVO model response in Figure 16(e) shows that the reflection from the base of the porosity is less dominant than in the P-P case. It is also apparent that the reflection from the top of the limestone interface is more dominant than in the P-P case. So, this detailed analysis of the P-SV AVO model response shows that there is less tuning overall. Furthermore, the degree of tuning at each interface is not consistent between the P-P and P-SV data as shown by the difference in relative strengths of the top of limestone and base of porosity reflections.

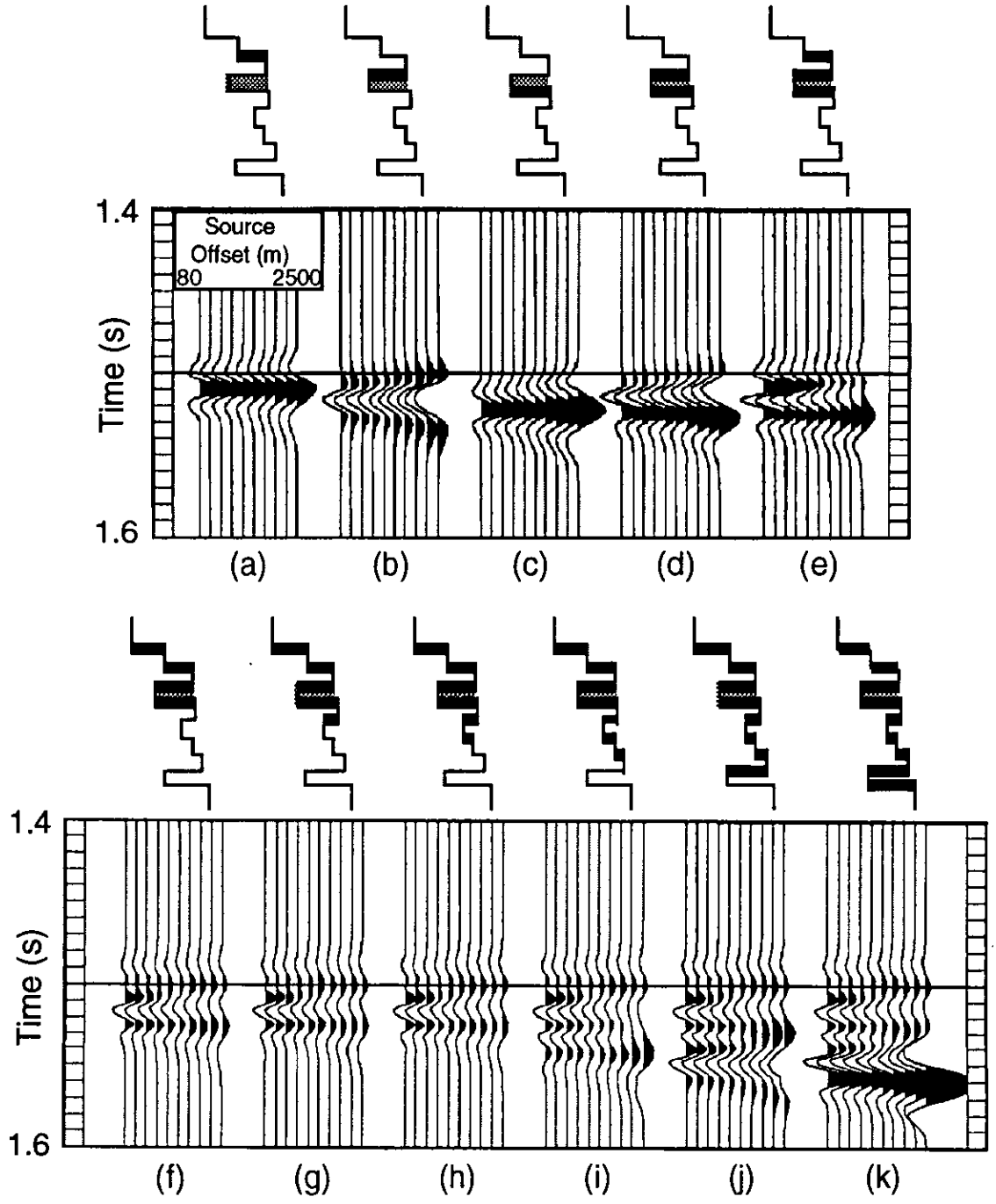

FIG. 15. P-P reflection forward models. Each model contains reflections from the highlighted reflector of the schematic impedance profile plotted above. The hatched area is the reservoir zone. (a) AVO model of the top of limestone interface. (b) AVO model of the top of the porosity interface. (c) AVO model of the base of porosity interface. (d) AVO model of the top and base of porosity interfaces. (d) AVO model of the top of limestone, top of porosity, and base of porosity interfaces. (e)-(k) AVO models of the highlighted interfaces.

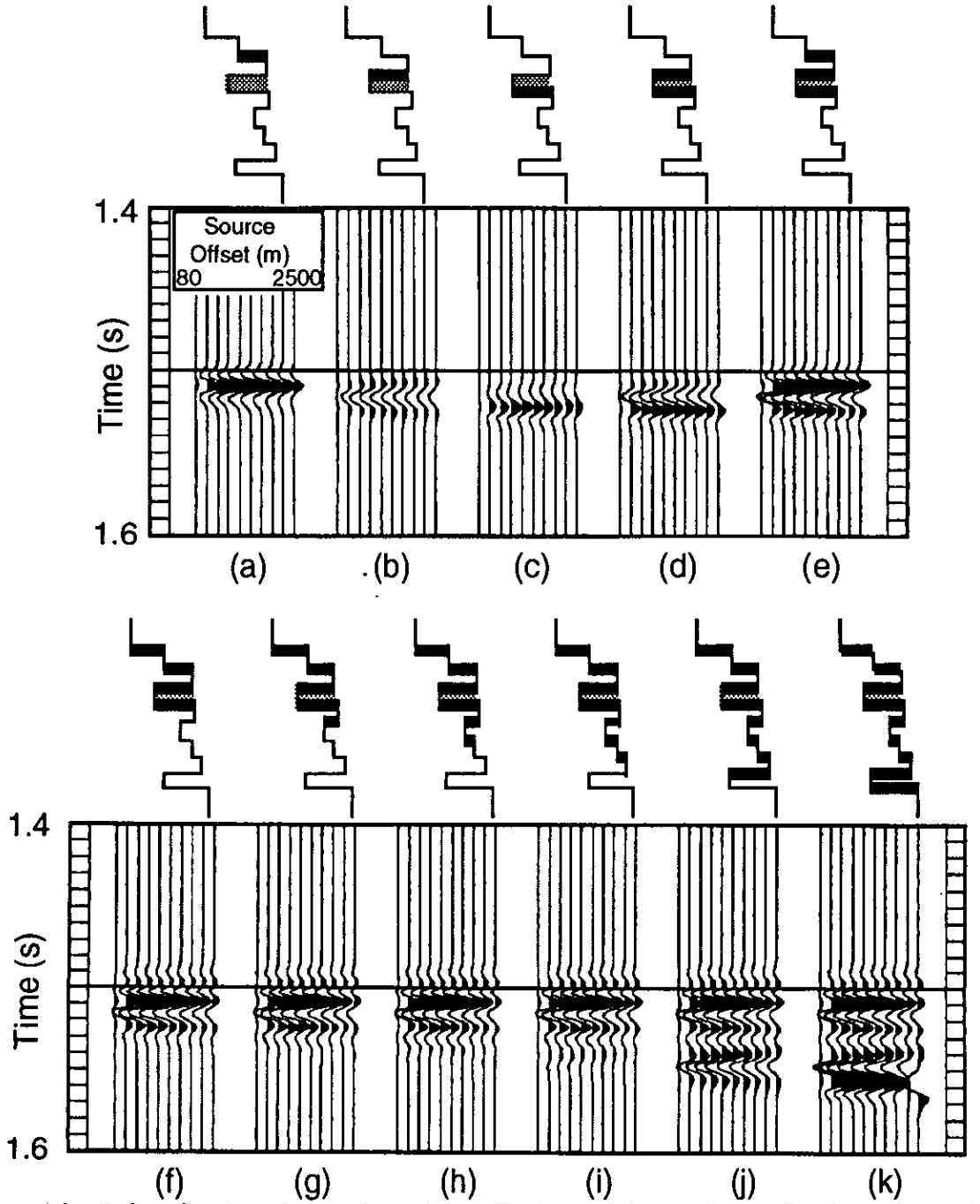

FIG. 16. P-S reflection forward models. Each model contains reflections from the highlighted reflector of the schematic impedance profile plotted above. The hatched area is the reservoir zone. (a) AVO model of the top of limestone interface. (b) AVO model of the top of the porosity interface. (c) AVO model of the base of porosity interface. (d) AVO model of the top and base of porosity interfaces. (d) AVO model of the top of limestone, top of porosity, and base of porosity interfaces. (e)-(k) AVO models of the highlighted interfaces.

The next step in the AVO analysis is to try to estimate the reservoir parameters from the VSP data. The approach used here is to visually compare the model and seismic responses and update the model until a better visual match is made. This approach is very qualitative in nature, and thus there is no guarantee that the match is better or the best match that can be found. Figure 17 and Figure 18 show the results of this analysis for the P-P and P-SV data respectively. The P-SV data have a lower signal to noise ratio than the P-P data, and the comparison of the field and model data (Figure 14) is better than the P-P data comparison. So, the P-P data will be emphasized for this analysis.

Four plots are shown in Figure 17. Figure 17(a) is the AVO forward model using a 100 Hz wavelet. This plot shows the largely untuned AVO response for the reservoir, and is used for event recognition. The top of porosity event in this plot is the trough at 1.517 s. Figure 17(b) is the AVO forward model using a 40 Hz wavelet. Figure 17(c) is the AVO forward model using a perturbed P-wave velocity in the porous-reservoir zone. Figure 17(d) is the field P-P gather. The P-wave velocity was lowered incrementally in the reservoir until a better qualitative match between the model and field data was found in the reservoir zone for the far offset traces. The velocity was lowered further until the AVO response deviated away from the field data. The final and perturbed velocities are listed in Table 3. So, a better model/field data match was obtained by perturbing the P-wave velocity in the reservoir zone. This raises the issue of justifying a change in the VSP velocities to obtain a better seismic reflection model.

Table 3. VSP and perturbed velocities.

Lithology	VSP Velocities			Perturbed Velocities		
	Vp (m/s)	Vs (m/s)	Vp/Vs	Vp (m/s)	Vs (m/s)	Vp/Vs
Limestone	5469	3026	1.81	5469	3026	1.81
Porosity	4817	2833	1.70	4333	2833	1.53
Limestone	5444	2937	1.85	5444	2937	1.85

The VSP interval velocities are determined from the traveltimes of the downgoing P and S wavefields. These traveltimes are measured in the borehole and thus are influenced by the rock volume within a finite radius of the borehole. The seismic reflections are influenced by a rock volume with a radius of 1/2 a fresnel zone around the borehole. So, the reflections are influenced by a larger rock volume than the downgoing wavefields. This suggests that any change in porosity, gas saturation, or other rock property away from the borehole will influence the reflected waves more than the direct arriving waves. Thus it is reasonable that the velocity model based on the VSP direct arrivals may be different from the velocity model based on the seismic reflections. It is also reasonable that the reservoir zone will be more heterogeneous away from the borehole than the other zones.

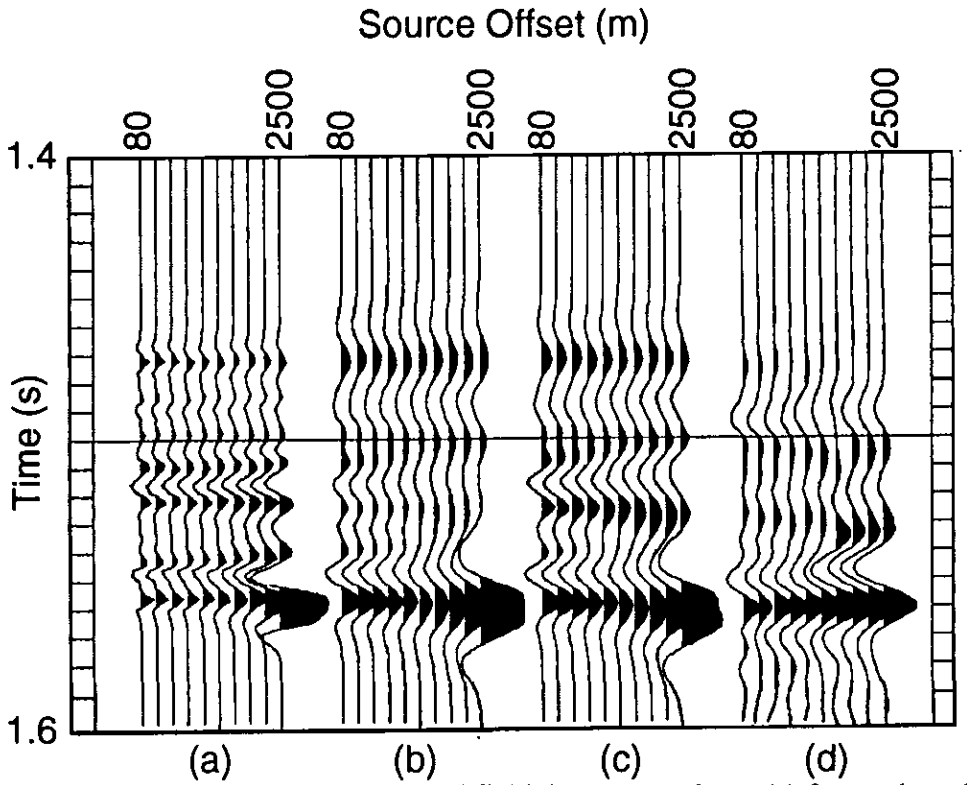

FIG. 17. P-P multilayer forward models and field data comparison; (a) forward model with 100 Hz wavelet, (b) forward model with 40 Hz wavelet, (c) perturbed model with 40 Hz wavelet, and (d) field P-wave gather.

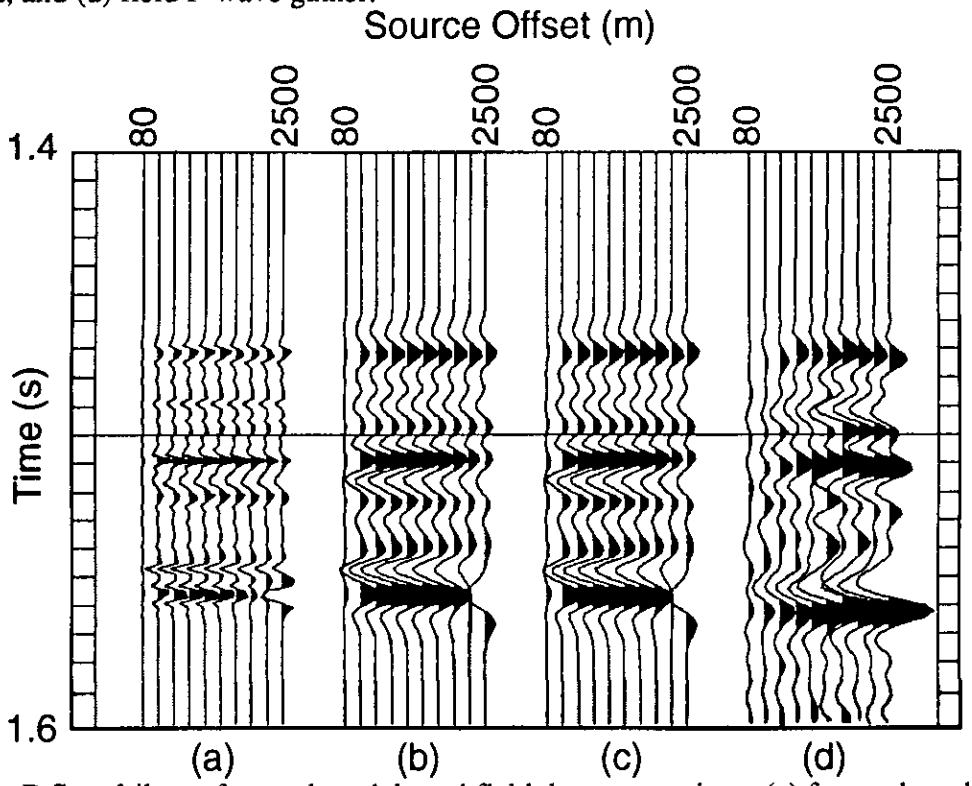

FIG. 18. P-S multilayer forward models and field data comparison; (a) forward model with 100 Hz wavelet, (b) forward model with 40 Hz wavelet, (c) perturbed model with 40 Hz wavelet, and (d) field S-wave gather.

CONCLUSIONS

Several different types of data have been used in this study to analyze the AVO response of a subsurface gas-bearing carbonate zone. The well log data were used to determine lithology, porosity, and rock properties. The reservoir zone is dolomitized with a porosity of about 15 %. The sonic and density logs were also used to forward model the 1-D synthetic and AVO response of the reservoir zone. There is a good correlation between the synthetic seismogram and zero-offset VSP corridor stack. A better correlation AVO response of the P-wave multioffset VSP field data and forward-modeled synthetic data was found by lowering the P-wave velocity in the reservoir zone.

REFERENCES

Aki, K., and Richards, P.G., 1980, Quantitative seismology: Theory and methods, V.1: W.H. Freeman and Co.

Chacko, S., 1989, Porosity identification using amplitude variations with offset: examples from South Samatra: Geophysics, 54, 942-951.

Cheng, S., Hron, F., and Daley, P.F., 1992, Determination of shear wave velocities from P-wave amplitudes in VSP data: J. Can. Soc. Expl. Geophys., 28, 19-29.

Dankbaar, J.W.M., 1987, Vertical seismic profiling separation of P and S waves: Geophys. Prosp., 35, 803-814.

Gaiser, J.E., DiSiena, J.P., and Fix, J.E., 1984, VSP: Fundamentals of the downgoing wavefield and applications that imporve CDP data interpretaion, in Toksoz, N.N., and Stewart, R. R., Eds., Vertical siesmic profiling Part B: Advanced concepts: Geophysical Press.

Geis, W.T., Stewart, R.R., Jones, M.J., and Katapodis, P.E., 1990, Processing, correlating, and interpreting converted shear waves from borehole data in southern Alberta: Geophysics, 55, 660-669.

Jolly, R.N., 1953, Deep-hole geophone study in Garvin County, Oklahoma: Geophysics, 18, 662-670.

Koefoed, O., 1955, On the effect of Poisson's ratios of rock strata on the reflection coefficients of plane waves: Geophys. Prosp., 3, 381-387.

Leaney, W.S., and Ulrych, T.J., 1987, Compound median filtering applied to sonic logs: 57th Ann. Int. Mtg. Soc. Expl. Geophys., Expanded Abstracts, 23-26.

Lee, M.W., and Balch, A.H., 1983, Computer processing of vertical seismic profile data: 48, 272-287.

Ostrander, W.J., 1984, Plane wave reflection coefficients for gas sands at non normal angles of incidence: Geophysics, 49, 1637-1648.

Rutherford, S.R., and Williams, R.H., 1989, Amplitude-versus-offset variations in gas sands: Geophysics, 54, 680-688.

Schlumberger, 1987, Log interpretation principles/applications: Schlumberger Educational Services.

Schlumberger, 1988, Log interpretation charts: Schlumberger Educational Services.

Stewart, R.R., 1984, Vertical-seismic-profile (VSP) inverval velocities from traveltime inversion. Geophys. Prosp., 32, 608-628.

Stewart, R.R., Huddleston, P.D., and Kan, K.T., 1984, Seismic versus sonic velocities: a vertical seismic profiling study: Geophysics, 49, 1153-1168.

Swan, H.W., 1991, Amplitude-versus-offset measurement errors in a finely layered medium: Geophysics, 56, 41-49.

Tatham, R.H., and Krug, E.H., 1985, Vp/Vs Interpretation: Developments in Geophysical Methods - 6., Ed. A.A. Fitch, Elsevier Applied Science Publications, London, New York.

Widess, M.B., 1973, How thin is a thin bed?: Geophysics, 38, 1176-1180.

Young, B.G., and Braile, L.W., 1976, A computer program for the application of Zoeppritz's amplitude equations and Knott's energy equations: Seismological Society of America Bulletin, 66, 1881-1885.